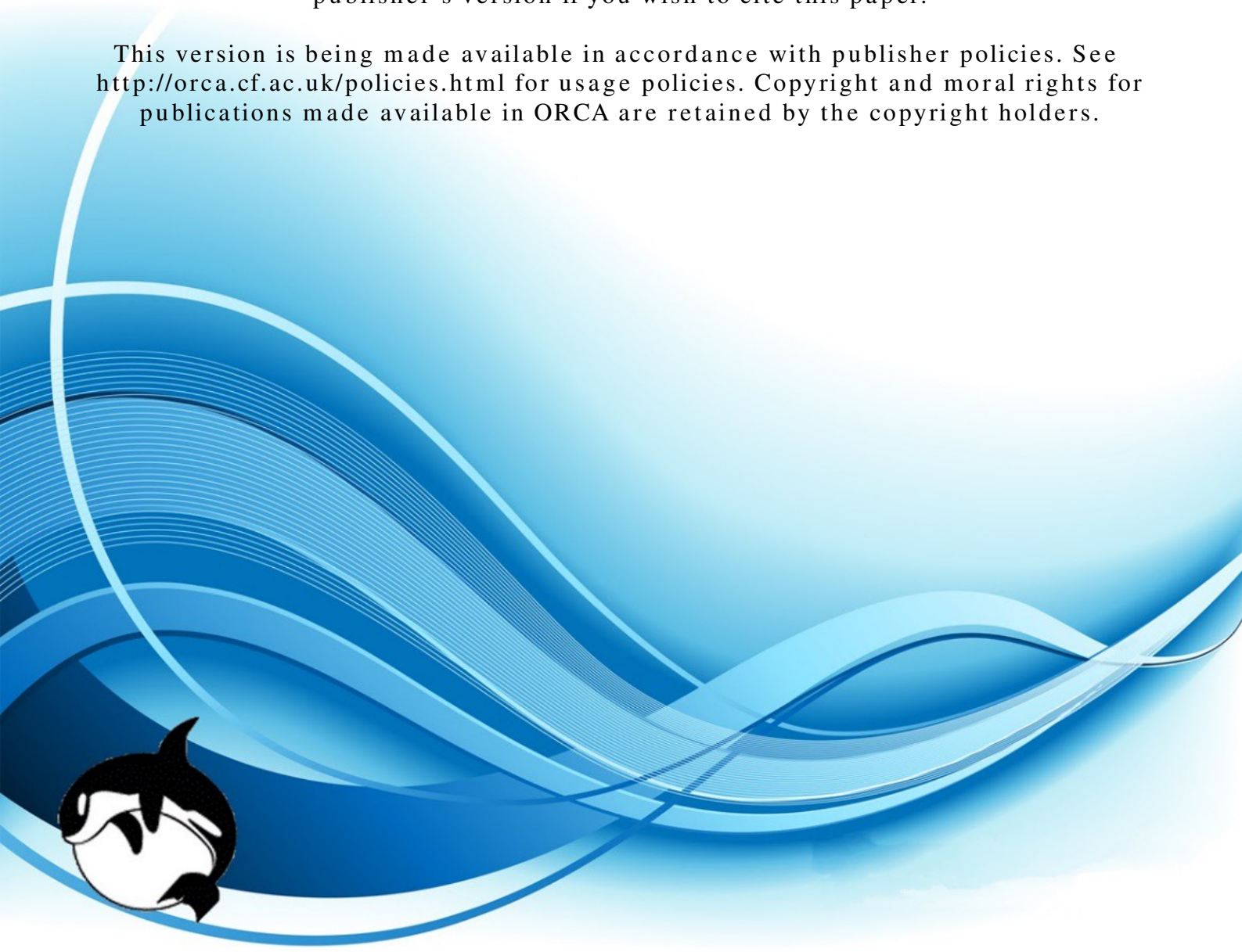

Optimisation of Acoustic Emission Wavestreaming for Structural Health Monitoring

John P. McCrory, Matthew R. Pearson, Rhys Pullin, Karen M. Holford

Cardiff University School of Engineering, The Parade, Cathays, Cardiff, UK, CF24 3AA

Abstract

Structural Health Monitoring (SHM) has gained wide appeal for applications with high inspection costs, such as aircraft and wind turbines. As the structures and materials used in these industries evolve, so too must the technologies used to monitor them. Acoustic Emission (AE) is a passive method of detecting damage which lends itself well to SHM. One form of AE monitoring, known as wavestreaming, involves intermittently recording data for set periods of time and using the sequential recordings to detect changes in the state of the structure. However, at present there is no standard method for selecting appropriate wavestream recording parameters, such as their length or their interval of collection. This paper investigates a method of optimising AE wavestreaming for SHM purposes by introducing the novel concept of adjoining consecutive discrete AE hit signals to create synthetic wavestreams. To this end, a pre-notched 492x67.5x20mm, 300M grade steel cantilever specimen was subject to a cyclic loading and both AE hit data and conventional wavestreams were collected as a crack grew in the notched region; crack growth activity was also monitored using Digital Image Correlation for comparison. To demonstrate the proposed optimisation process, four sets of synthetic wavestreams were created from the hit data, 0.25, 0.5, 1.0, and 1.5 seconds in length, and compared with the 1.5 second long conventional wavestreams. The activity of the peak frequency and frequency centroid bands of interest within the conventional and synthetic wavestreams were examined to determine whether or not cracking activity could be inferred through them. Across comparisons of all data it was found that the 0.5 second long synthetic wavestreams contained enough information to identify the same trends as the conventional wavestreams for this application, thus the use of synthetic wavestreams as a tool for selecting an appropriate wavestream recording length was demonstrated.

Keywords: Structural Health Monitoring, Acoustic Emission, Wavestreaming, Optimisation, Fatigue, Cracking

Introduction

Structural Health Monitoring (SHM) is the process of collecting information about the state of a structure or component, often through the use of embedded or mounted sensors. This information can inform the operator of any faults or structural issues, giving an early warning before catastrophic failure. Operators of structures, such as aircraft and offshore wind turbine, which currently undergo rigorous scheduled maintenance inspections could reduce their asset downtime and associated operating costs by implementing SHM [1–3]. As well as the immediate financial and safety benefits, through the collection of more comprehensive diagnostic information, an SHM system could influence and inform future designs by identifying problem areas and features. Looking further ahead, the case could be made that if the use of SHM systems became widespread and trusted, they could eventually lead to structures being designed with lower factors of safety, which would reduce material use, mass and consequently, in the case of aviation and transport, reduce fuel consumption and thus environmentally harmful emissions. Whilst a fully autonomous and sophisticated SHM system has yet to be realised, there is ongoing research on numerous fronts in order to make this happen including; energy harvesting; power storage and management; wireless communications; and damage detection. With regards to damage detection, Acoustic Emission (AE) is a technique which uses piezoelectric transducers to measure the transient elastic energy released by damage as it initiates and propagates [4]. Unlike many other, conventional NDT techniques which rely on actively sending a signal into the structure, AE is a passive technique, utilising the signals released by the structure itself; thus AE lends itself well to SHM applications as it allows in situ global monitoring of structures. By using an array of AE sensors, the time of arrival of signals at each sensor can be compared in order to calculate the location of the source of the emission. Furthermore, the signals detected by AE sensors can be recorded and scrutinised in order to determine information about their source, in a process known as characterisation.

Whilst AE is now being implemented in an industrial capacity for monitoring and inspecting bridges [5]; gas trailer tubes [6]; pressure vessels [7]; welded joints [8]; and offshore platforms [9], there are many more potential applications offering benefit to the industry adopting the technology. Particular benefit could be seen for safety critical structures which require ongoing periodic inspection, such as aircraft, and structures which are difficult to access and monitor, such as offshore wind turbines. However, certain challenges exist which act as barriers to the adoption of AE in these fields. Technical challenges still exist in the sense that the ability to locate events using AE is severely hampered in complex structures due to the complexity of the wave propagation and signal attenuation. Practical challenges also need to be resolved, such as the development of an AE based SHM system with low enough power requirements that it can be powered via harvested energy, for applications where the use of batteries is either prohibited or highly discouraged. This is particularly challenging considering that the current low-power AE systems available on the market are rated at 6W [10] and, depending on the available sources, practically sized energy harvesting technologies are far from this capacity [11,12].

With this in mind, wavestreaming should be considered as a potential low-power format of AE monitoring as data is captured periodically, thus allowing down time for energy harvesting to generate power. Wavestreaming is a form of AE data collection whereby all of the data collected on each AE channel is recorded for a set period of time, regardless of the signal amplitude. This is contrary to the more conventional hit based monitoring, whereby AE data is only recorded if the amplitude of the signal on a channel exceeds a certain threshold, Figure 1.

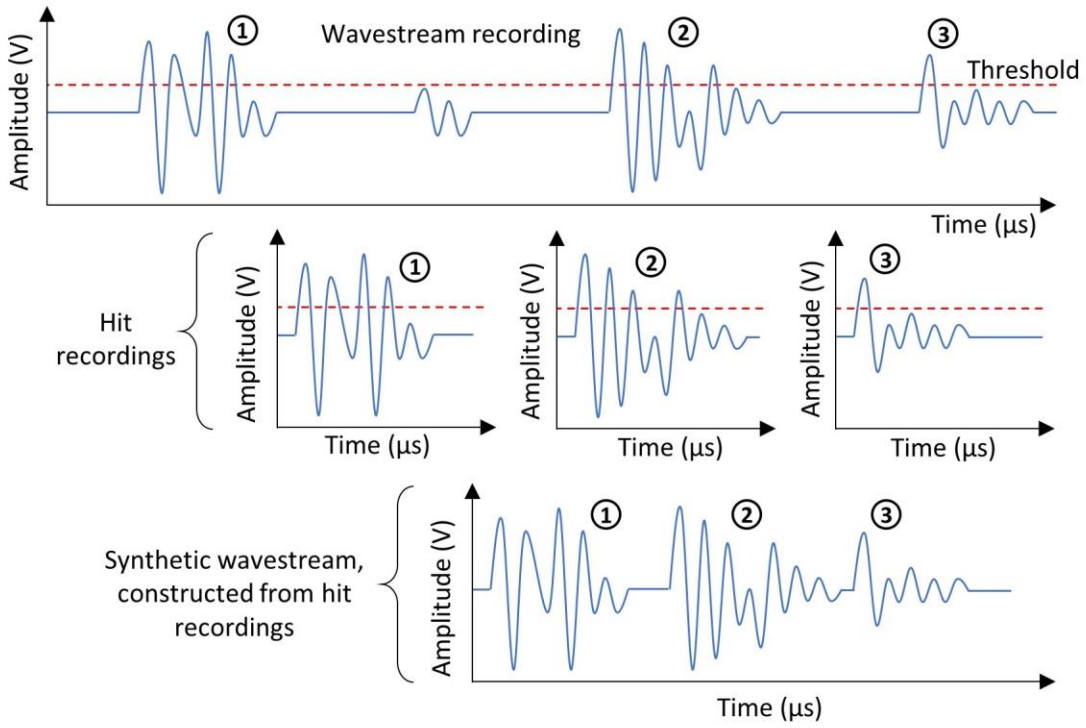

Figure 1: Representation of conventional wavestreaming, hit based recording, and synthetic wavestream creation

Wavestreaming has attracted the attention of researchers due to its ability to capture continuous processes. Following on from a similar study by Mascaro et al. [13], Eaton et al. [14] used wavestreaming to monitor the drilling process in a carbon fibre panel; the RMS of the wavestreams was used as an indicator to track the progression of wear in the tool and also the condition of the hole being drilled. Wavestreaming has been employed to good effect in the field of rotating machinery, with numerous studies using a comparison of successively captured wavestreams to detect the changing condition of gears and bearings [15–19]. As well as detecting the presence of damage, efforts have also been made to extract information about the severity of damage from wavestream recordings. Elforjani and Mba [20] elegantly calculated the size of a ball bearing race defect by measuring the length of the transient AE occurring in wavestreams collected as the bearing rotated at a known angular velocity. Eftekharnejad et al. [21] discovered changes in the frequency content of decomposed AE wavestreams before and after shaft fracture occurred in an experiment on a gearbox, demonstrating how wavestream frequency domain information can assist in providing diagnostic information. There are also examples of the use of wavestreaming to investigate non-rotating, cyclically loaded structures. Pullin et al. [22] and Holford et al. [23,24] looked at the potential of using cross-correlation and frequency information to track the presence and progression of damage in a static gear tooth load test. Pullin et al. [25] also used a banded frequency analysis on wavestream recordings to identify the presence of delamination damage in cyclically loaded a carbon fibre panel. More recently Zhang et al. [26] used a windowed decomposition of wavestream recordings in order to detect variations in the peak frequency and frequency centroid values, thus identifying cracking signals recorded in the spline testing of the helicopter gearbox. The bodies of work touched upon here show that wavestreaming is a diverse tool, providing rich data sets which can assist research.

In the context of SHM, wavestream data can be used to detect differences in the structure's acoustic fingerprint, which may be an indicator of damage or change in the structure. It follows that by collecting wavestreams periodically over a structure's lifetime, the deterioration of that structure

should be visible by comparing features of the consecutively collected wavestreams, due to the presence of signals emitted by evolving damage sources. In order to enable this, appropriate recording intervals and wavestream recording lengths need to be established for each application; if the wavestreams are too short or sparsely collected then detection of the onset and evolution of damage might be delayed or missed, whilst unnecessarily long and frequent wavestream recordings will result in a more power hungry system incompatible with the requirement for a low power SHM system. However, at present there is no standard method for selecting these parameters; instead they are selected at the discretion of the user. This study introduces the concept of synthetic wavestreams, which could provide a method of selecting the appropriate wavestream recording parameters for real world SHM applications.

A synthetic wavestream is the term introduced in this paper to describe the data set created by adjoining consecutively recorded AE hits in order to produce a longer, conjugated signal, which is analogous to a conventional wavestream recording. The way in which an synthetic wavestream differs to a conventional wavestream is that it does not contain all of the periods of noise in between the hit signals embedded within a conventional wavestream, instead it consists solely of these hit signals, as demonstrated in Figure 1. As suggested, one of the purposes of looking at the data in this way is that it could prove to be a useful tool for selecting appropriate wavestream collection parameters; namely the length and interval of collection. For instance, if AE hit data is collected as a component is fatigued to failure, synthetic wavestreams can subsequently be created from that hit data. It is suggested that several synthetic wavestream data sets could be created, each using the hits occurring within a different length time window, i.e. different length synthetic wavestreams. These synthetic wavestream data sets can then be analysed to see which contain enough relevant information to promptly detect structural degradation, and thus an appropriate length wavestream can be suggested for use on this component going forward, which is optimal for the application. The wavestream recording interval could also be investigated by creating synthetic wavestream data sets with different intervals of creation and, again, determining which are capable of detecting structural degradation in a timely manner.

In this paper, the AE data collected during a fatigue test on a cantilevered steel specimen will be used to demonstrate this process. Synthetic wavestreams of varying lengths will be created and compared against the conventional wavestreams. To this end the optimum length wavestream recording will be established for this hypothetical monitoring application.

Experimental Procedure

A fatigue experiment was designed using a 492x67.5x20 mm, 300M grade steel beam specimen. A notch was cut in the specimen with a wire cutter, in order to accelerate cracking. The specimen, and notch dimensions are shown in Figure 2.

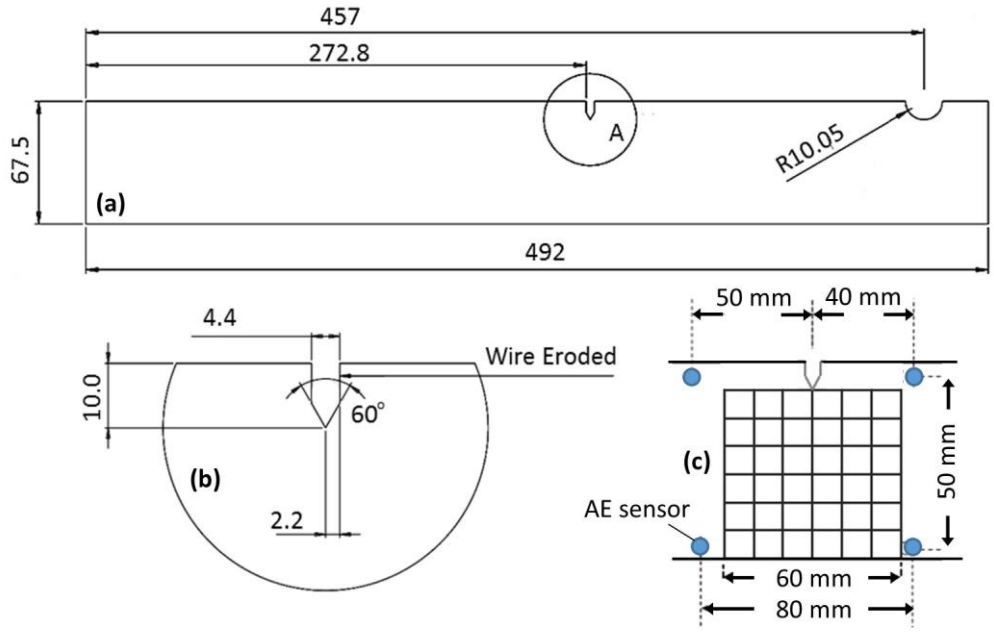

Figure 2: (a) Steel specimen used for the test, (b) details of the notched region, and (c) the positions of the AE sensors relative to the notch

The presence of the notch also simplifies the task of placing the AE sensors, as the damage region is known in advance. Thus, four Mistras Nano30 AE sensors (125-750 kHz) were bonded to the surface of the specimen in the region around the notch, as shown in Figure 2(c). The sensors were bonded using Loctite595 silicone sealant, which also served as the acoustic couplant between the sensors and the specimen. The sensors were connected to a Mistras PCI2 based AE acquisition system through Mistras pre-amplifiers, set to 60dB amplification and with a built in bandpass frequency filter of 20-1200 kHz. A 60x60 mm grid, with 10mm grid spacing, was drawn on to the surface for the purposes of the Delta-T Mapping, which is a location algorithm which has been shown to provide improvements in accuracy when compared to the traditional Time of Arrival method [27,28]. A full description of Delta-T Mapping and its implementation can be found in the works of Baxter [29] and Pearson [30]. The reverse side of the specimen was prepared for Digital Image Correlation (DIC) by using spray paint to apply a black and white speckle pattern.

Once specimen preparations were complete, the leftmost end of the specimen was placed on a block and clamped rigidly to the bed of the test machine, such that the remainder of the specimen was left in a cantilever arrangement, as represented in the schematic diagram shown in Figure 3. The circular notch was fitted with a 20 mm long, 20 mm ø roller pin to allow load transfer via a uniaxial testing machine, and the actuator head of the load machine was brought into contract with the roller. A cyclic compressive load between 0.5 and 11 kN was applied to the roller at a rate of 1Hz, in order to put the specimen into bending and promote crack growth in the notched region. The specimen was loaded for 67,000 cycles until a sufficiently long crack was evident through visual observation.

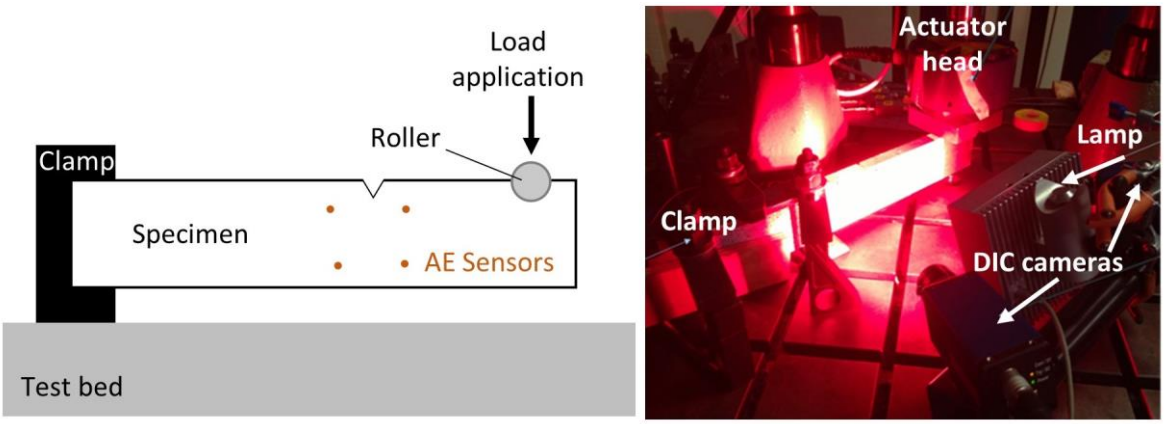

Figure 3: Experimental setup

A two 2-Megapixel camera Dantec Dynamics DIC system was set up to monitor the region of the notch, also shown in Figure 3. During loading, classic AE hit data was monitored using the acquisition settings listed in Table 1, and 1.5 second long wavestreams were recorded every 500 loading cycles. Furthermore, after every 500 cycles the load was held at 11kN for an image to be taken using the DIC system, hence the collection intervals of the wavestreams and DIC data were in sync.

Table 1: Acquisition settings used within AEWin (PDT-Peak Definition Time, HDT-Hit Definition Time, HLT-Hit Lockout Time)

Threshold (db)	Filter (kHz)	Sample rate (kHz)	Length (ms)	Pre-trigger (ms)	PDT (ms)	HDT (ms)	HLT (ms)
40	20-1200	2000	1.5	0.5	0.2	0.4	1

Results and discussion

Using a similar approach as those taken by Reu et al. [31] and Lemmen et al. [32], crack growth was determined using DIC by tracking the strain field in the region of the crack tip. The strain values from all of the subsets along the length of the crack were exported for every image captured, Figure 4(a). The strain data for each image was then investigated to identify the first subset along the line of the crack with a strain value in excess of the 0.2% yield strain criteria [33]. Whilst it does not give the crack's exact length, tracking the movement and relative depth of the plastic region around the crack tip gives a good indication of growth rate. Further to this, an indication of the instantaneous crack growth was gained by fitting a smoothing spline to the data and calculating the incremental movement of the plastic region from one image to the next, Figure 4(b).

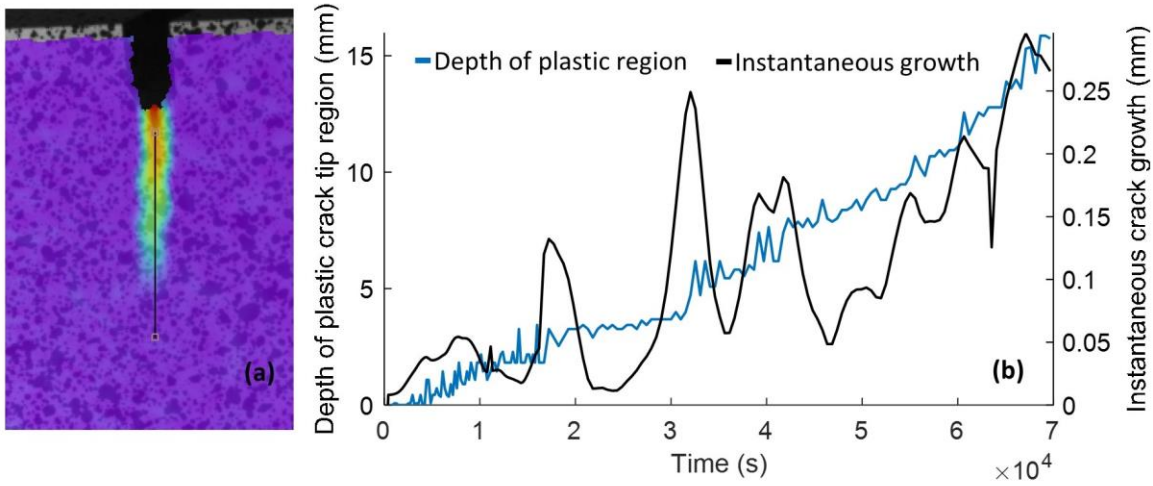

Figure 4: (a) Example of DIC data selection within Dantec Istra4D software (b) DIC data showing the position of the 0.2% strain region relative to the notch tip over the duration of the experiment (blue), and the incremental movement of the 0.2% strain region from one image to the next (black)

From the curves shown in Figure 4(b), it can be observed that the crack growth rate changes over the duration of the test, with the overarching trend showing an increase in crack growth rate as the test progresses, indicated by the steadily increasing gradient of the blue curve and the larger instantaneous movements of the plastic region in front of the crack tip from one image to the next. This is expected, as classic fatigue cracking theory states that larger crack lengths result in larger growth rates [34]. The stochastic instantaneous crack growth from one image to the next shows somewhat typical fatigue behaviour, with periods of crack growth followed by periods of crack arrest [35–37]. It should be noted that continuous loading of the specimen was interrupted many times during the test so that an image could be captured for DIC analysis, during which time the specimen was held at the maximum load. Since the fatigue crack growth mechanism is a delicate process, relying on the movement of slip planes in the regions of plastic deformation around the crack tip [36], these interruptions to the loading conditions will have acted to disrupt this process, contributing to the slightly sporadic nature of the crack growth observed [38]. Classical AE parameters can be used to infer some information about the experiment and state of cracking in the structure. Figure 5(a) shows the cumulative number of hits recorded by channel 1 near the beginning of the test; the rate of AE release increases at approximately 7500 seconds, indicating that this is the point at which AE begins to indicate significant activity due to crack growth. This finding was supported by investigating the rate of occurrence and location of AE events, which were located using Delta-T Mapping, Figure 6. There are far more AE events located between 7300 and 8350 seconds than there are between 0 and 7000 seconds. Furthermore, the events located between 7000 and 8350 seconds are more concentrated in the region of the notch, thus giving more weight to the argument that AE began to indicate significant crack growth activity at approximately 7500 seconds. However, the cumulative hits and cumulative energy curves shown in Figure 5(b) display the limitations of these simple measures since, in the broader context of the experiment, neither of these curves align well with the crack growth rate obtained from the DIC (the spline smoothed DIC data shown here for ease of comparison). The majority of the instances at which the crack growth rate changes are not reflected with corresponding changes in rate of increase of either the cumulative hits or energy, thus these parameters by themselves would not accurately inform an operator of the rate of crack growth in the structure, hence why more sophisticated analyses are required.

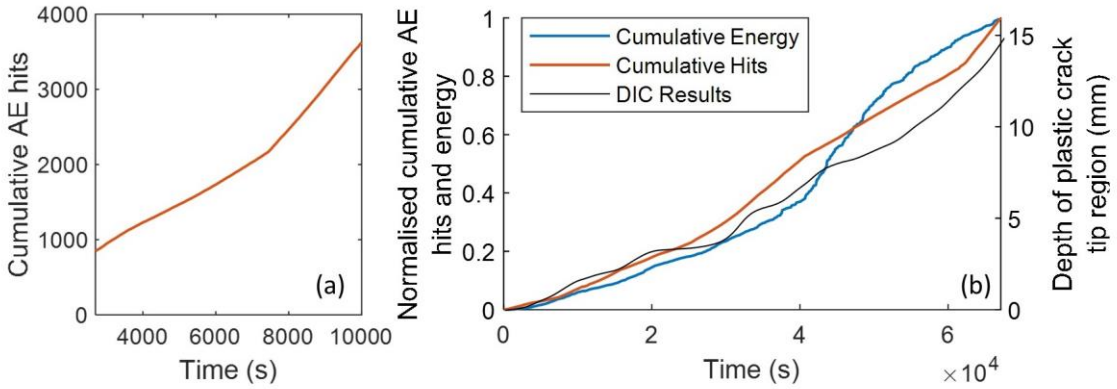

Figure 5: (a) a zoomed in image of the cumulative hits against time graph for Channel 1 (b) Normalised cumulative energy and hits for all AE on Channel 1, alongside the depth of the plastic region as calculated from DIC

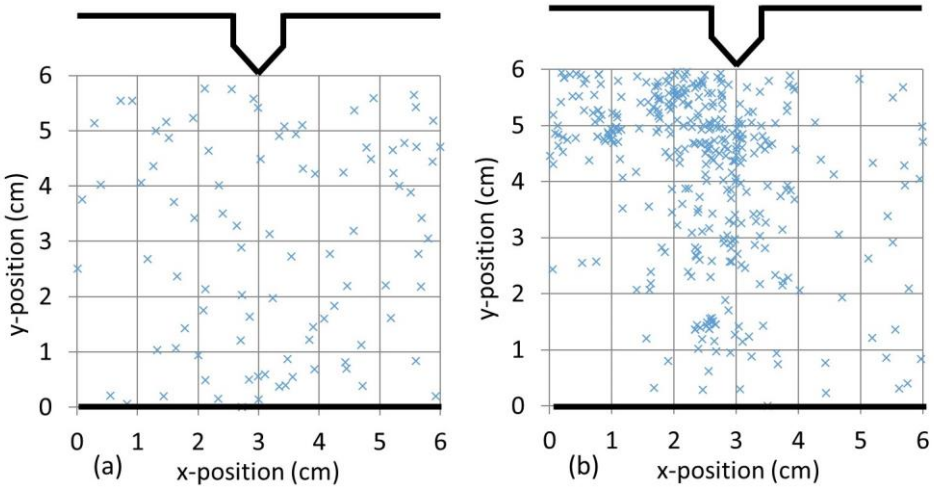

Figure 6: Locations of events calculated using Delta-T Mapping between (a) 0 and 7000 seconds and (b) 7300 to 8350 seconds

A common practice in AE is to study located signals to determine the characteristics of emissions released by certain damage mechanisms. To this end, the largest amplitude events occurring during this experiment and located as originating from the notch tip region were investigated in order to determine the nature of AE from crack growth, as it is considered that the crack growth mechanism has the potential to produce the highest amplitude activity due to the amount of energy released as two new surfaces are formed [39,40]. An example of the waveforms recorded from these events and their associated frequency spectra is shown in Figure 7.

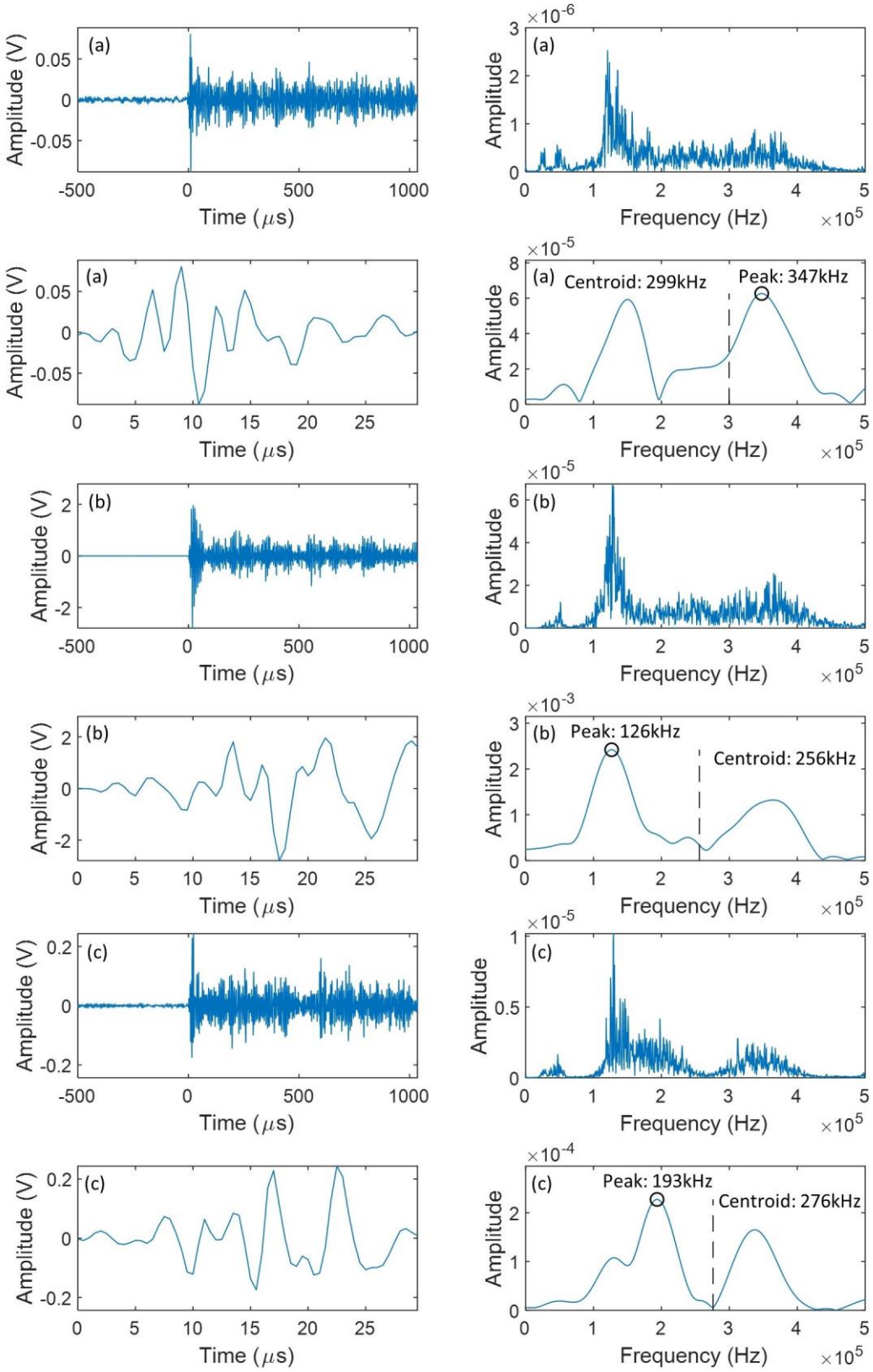

Figure 7: Full waveform and its frequency spectra, and the first 30µs of the same signal and its frequency spectra for (a) 59dB event occurring at 8,070 seconds, (b) 88dB event occurring at 10,029 seconds, and (c) 67dB event occurring at 65,440 seconds. All waveforms recorded on Channel 1

When looking at the frequency spectra of the entire wave, the majority of the energy is contained between 100-150kHz. However, if you take only the first arrival of the wave, the first 30µs in this instance, then a different pattern emerges; the relative amplitude of 300-400kHz frequency band increases to levels comparable with that of the 100-150kHz band. In this experiment, the first arrival of the wave is the truest representation of the energy released by the source as it is uncorrupted by the reflections and sensor ringdown which are prevalent in the tail end of the signal, thus, it could be inferred from the results shown in Figure 7 that the cracking process releases AE with a strong 300-400 kHz frequency component. This is in keeping with the literature which suggests that cracking is known to induce stronger high frequency content [41,42] and in a similar frequency range to this [43]; though it should also be noted that this is a frequency range at which the sensors have a particularly strong response.

To investigate this further, and in keeping with the work of other researchers [26], two quantities were examined; the peak frequency and the frequency centroid. The frequency centroid is calculated using Equation 1, where x_n is the centroid frequency of band n, and f_n is the amplitude of that band:

$$\frac{\sum f_n x_n}{\sum f_n} \qquad \textit{Equation 1}$$

As can be seen in Figure 7, the peak frequency of the first arrival of these signals is inconsistent; falling between 300-400 kHz in some instances though not in others. Unlike the peak frequency, which is dictated by a single value, the frequency centroid takes into account the entire spectrum, weighted by its relative amplitude. Thus, the effect of the prominent 300-400kHz band will always have a bearing on the calculation of the frequency centroid, meaning that it could be a more reliable quantity by which to identify these signals. This can be seen in Figure 7, where the signals consistently have a frequency centroid value between 250-300kHz. Whilst it is possible for the frequency produced by crack growth activity to change over the course of the experiment as the mechanism of crack growth itself changes [44], the high amplitude signals investigated here were taken from various points in the test adding some confidence to the fact that this frequency band will remain relatively consistent. Thus, the activity of the 250-300 kHz frequency centroid band identified here will be investigated in the ensuing analysis of the wavestreams and synthetic wavestreams, to determine whether it is able to be used as a descriptor of crack growth activity.

As well as primary signals from crack growth itself, secondary signals, such as those from crack-face rubbing, can be valuable indicators of crack activity [45]. It is understood that crack face rubbing signals are typically lower amplitude than crack growth signals and can occur at a range of amplitudes during a single test [42,45,46]. It is therefore challenging to attempt to isolate crack face rubbing signals in this experiment based on amplitude and location, however there are discussions of crack-face rubbing in the literature from which to draw upon. Noting that the frequency of a signal recorded by an acquisition system is dependent on the transfer function of the signal from the source, including material and geometric effects, and sensor and preamplifier characteristics, it can be difficult to compare the results found in various literature on characterisation of mechanisms using frequency with high precision. Despite this, there is a strong consensus across multiple sources that signals relating to crack-face rubbing are characterised by low frequencies [47] particularly by peak frequencies in the region of 30-100 kHz [42,43,45] and a frequency centroid of 160-175 kHz [46]. Thus, consideration will also be paid to these peak frequency and frequency centroid bands in the wavestream analysis.

Synthetic wavestreams corresponding to each of the conventional wavestreams were created by sequentially adjoining the hits which occurred in the same time window as the wavestream recordings. To demonstrate the optimisation process proposed in this paper, four synthetic wavestream data sets were created using 0.25, 0.5, 1.0, and 1.5 seconds worth of hit data respectively, i.e. the 1.5 second long synthetic wavestreams consists of all the hits captured in the same time period as the 1.5 seconds long conventional wavestreams, but without the periods of low activity noise between hits, whereas the 0.25 second long synthetic wavestreams contains only the hits occurring within the first 0.25 seconds of the conventional wavestreams. Examples of conventional wavestream recordings and their associated synthetic wavestreams of different length are shown in Figure 8 for two different stages of the test.

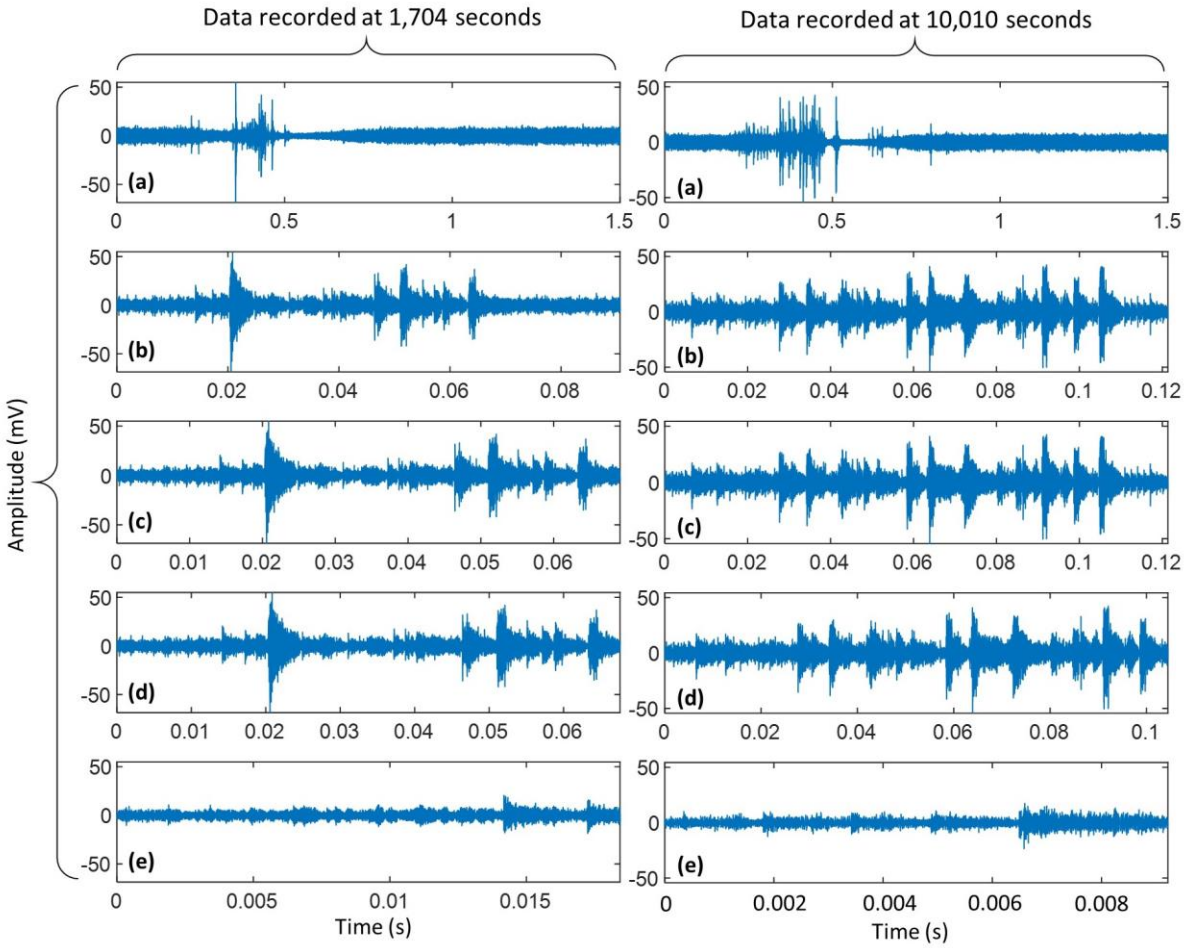

Figure 8: Examples of conventional wavestream recordings (a), and synthetic wavestreams created from 1.5 seconds worth of hits (b), 1.0 seconds worth of hits (c), 0.5 seconds worth of hits (d), and 0.25 seconds worth of hits (e)

It can be seen that the wavestream recorded at 1,704 seconds into the test has significantly less higher-amplitude transient activity than the wavestream recorded at 10,010 seconds into the test. This is to be expected following that significant crack growth activity isn't thought to have begun until approximately 7,500 seconds into the test. The synthetic wavestreams display a predictable tendency, with the 1.5 second long synthetic wavestream containing more information than the shorter length synthetic wavestreams, though still containing less data points than the conventional wavestream, due to the lack of presence of any data not belonging to a hit. Interestingly, there are two examples in Figure 8 where two different length synthetic wavestreams contain very similar amounts of data; (c) and (d) for the 1,704 second recording, and (b) and (c) for the 10,010 second recording. These

instances give a precursor as to the purpose of synthetic wavestream as a tool for selecting the correct wavestream recording length, since it visualises how the same effective data can be received despite a shorter time recording window. Following the trend seen in the conventional wavestreams, the synthetic wavestreams created from the data captured at 10,010 seconds into the test contain more transient signals than the synthetic wavestreams of the same length created from the data collected at 1,704 seconds into the test. To visualise this for the entirety of the test, Figure 9 shows a plot of the number of hit signals contained within each of the different length synthetic wavestreams. There are periods where the number of hits contained between the different length synthetic wavestreams is comparable and periods where there is a large variation. Despite differences in the values themselves, similar trends in the number of hits over the duration of the test can be seen in all of the different length synthetic wavestreams, though the 0.25 second long synthetic wavestream bears the least resemblance, especially during the first 20,000 seconds of the test.

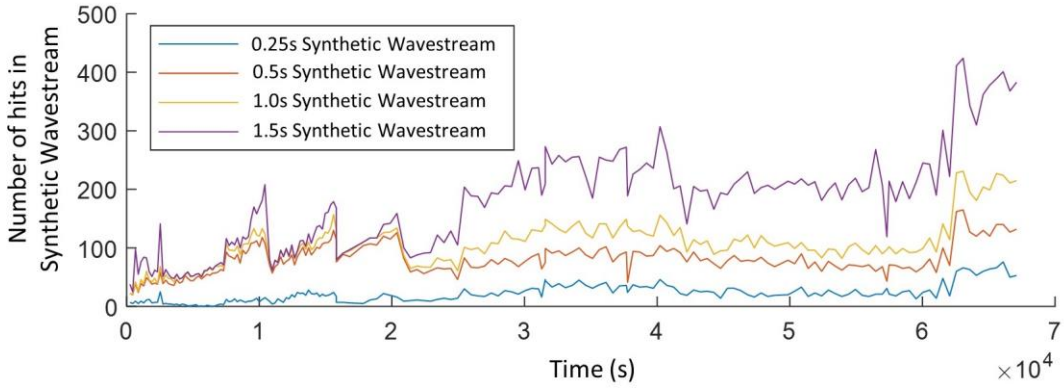

Figure 9: Number of hits captured in each of the different length synthetic wavestreams

The following analysis assess the trends in the different length synthetic wavestreams and how they compare with those in the conventional wavestream recordings, in order to determine the minimum length wavestream recording that is still able to portray relevant information about the state of the structure. To this end, Figure 10 shows the RMS amplitude of each of the synthetic wavestreams plotted against the RMS amplitude of the conventional wavestreams. It can be noted that the majority of the synthetic wavestream recordings have larger RMS amplitudes than the conventional wavestream recordings; this is to be expected as the conventional wavestream recording RMS amplitude is diluted by the vast periods of noise captured between transient events. Of more consequence are the trends seen within the amplitudes. As expected, as the length of the synthetic wavestream recording length reduces, so too does its semblance to the conventional wavestream recording. Nearly all of the peaks and troughs in the RMS amplitude of the conventional wavestreams are mirrored by peaks and troughs in the 1.5 second long synthetic wavestream; however, as the length of the synthetic wavestream is reduced, more of these peaks are missed. Generally speaking, the trends in the RMS amplitude seen within the conventional wavestream recordings are visible within the 0.5, 1.0, and 1.5 second long wavestreams, though the 0.25 second long synthetic wavestream fails to display the same behaviour; this is the first indication of what could be considered to be suitable wavestream recording lengths.

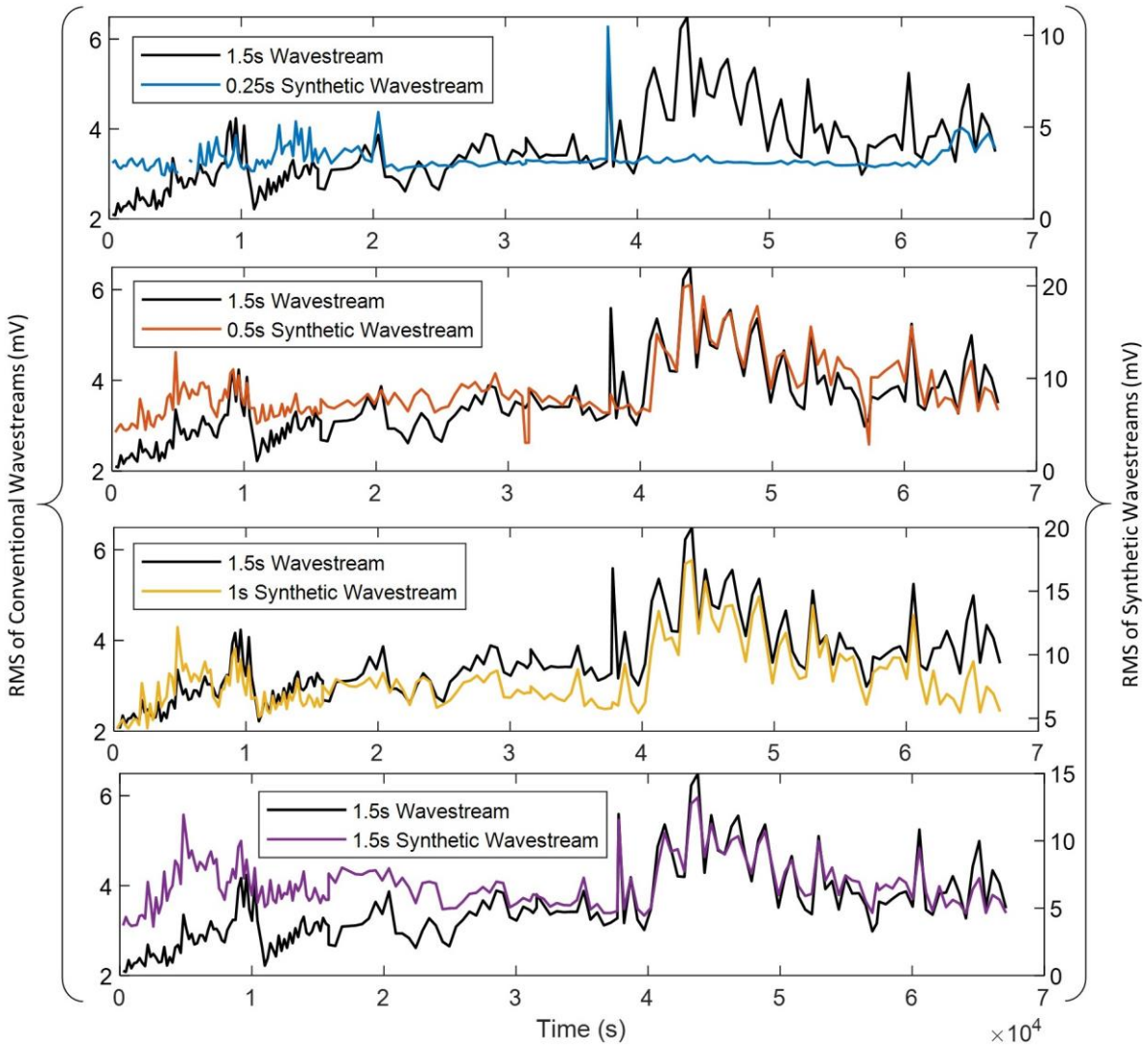

Figure 10: RMS amplitude of each synthetic wavestream alongside the RMS amplitude of the conventional wavestream

Inspired by the analysis of Zhang et al. [26], each wavestream and synthetic wavestream was analysed spectrally using a moving time window. Each data set was split into 30µs time steps, corresponding to the length of a transient signals identified previously, Figure 7. For each time step the spectrum was calculated, after the application of 40% Tukey window, allowing the peak frequency and frequency centroid of that time step to be determined. Figure 11 contains a visual representation of the results of this process for one synthetic wavestream alongside the corresponding conventional wavestream, at two points in the test. It can be seen that the peak frequency of the majority of the time bins fall inside two main bands centred around 30 kHz and 130 kHz. Both of these peak frequency bands are present for the entirety of each of the recordings, even during periods of low amplitude activity, implying that they are the product of a source of continuous or recurring emission, or background noise in this test. Occurring more sparsely in the wavestream recorded at 1,704 seconds into the test than the wavestream recorded at 10,010 seconds into the test are time bins with peak frequencies above 200 kHz; these correspond with the periods of high amplitude transient activity. The frequency centroid data tells a similar story, with the majority of time bins having a similar frequency centroid, centred around 200 kHz, but with periods of elevated frequency centroid corresponding to the periods of higher-amplitude transient activity.

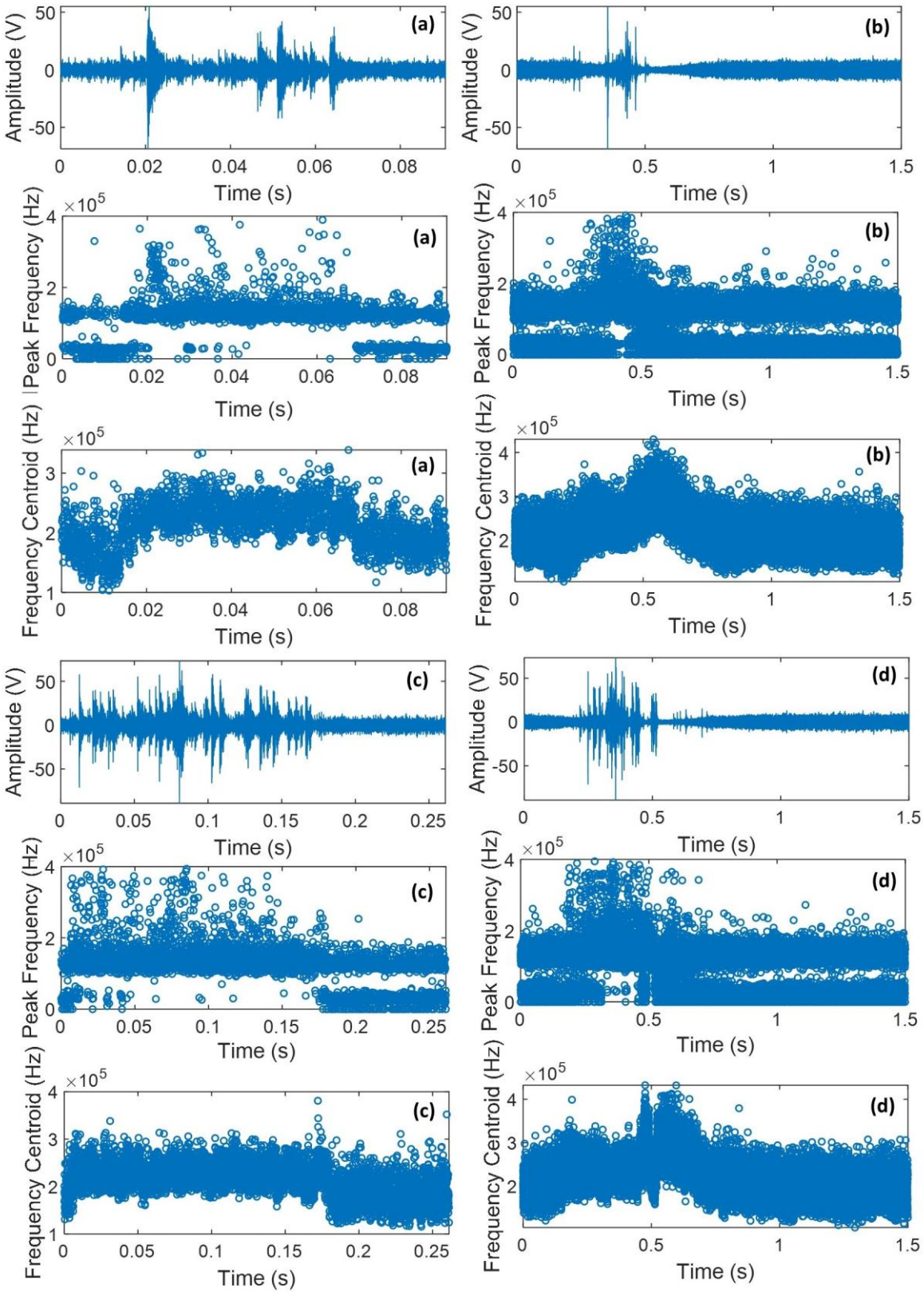

Figure 11: Plot of the wavestream signal, the peak frequency of each time bin within that wavestream, and the frequency centroid of each time bin within that wavestream for (a) 1.5 second long synthetic wavestream at 1,704 seconds into the test, (b) 1.5 second long conventional wavestream from 1,704 into the test, (c) 1.5 second long synthetic wavestream at 10,010 seconds into the test, (d) 1.5 second long conventional wavestream at 10,010 seconds into the test

A method of scrutinising this data over the duration of the test was required in order to compare the trends seen in the different length synthetic wavestreams with the conventional wavestream, as well as investigate the suitability of using the frequency bands identified previously as a measure of crack growth activity. Thus, the number of occurrences of time steps with peak frequency and frequency centroid values in 50 kHz frequency bands were summed for each wavestream and synthetic wavestream; this allowed the relative amount of activity in these bands to be tracked throughout the entirety of the test. Tracking the activity of different frequency bands is a popular method of attempting to distinguish between background noise, which is not expected to evolve with time, and AE from relevant sources relating to crack growth, which are expected to evolve with time [48]. The cumulative activity of all 50 kHz peak frequency and frequency centroid bands for the 1.5 second long synthetic wavestreams can be seen in Figure 12.

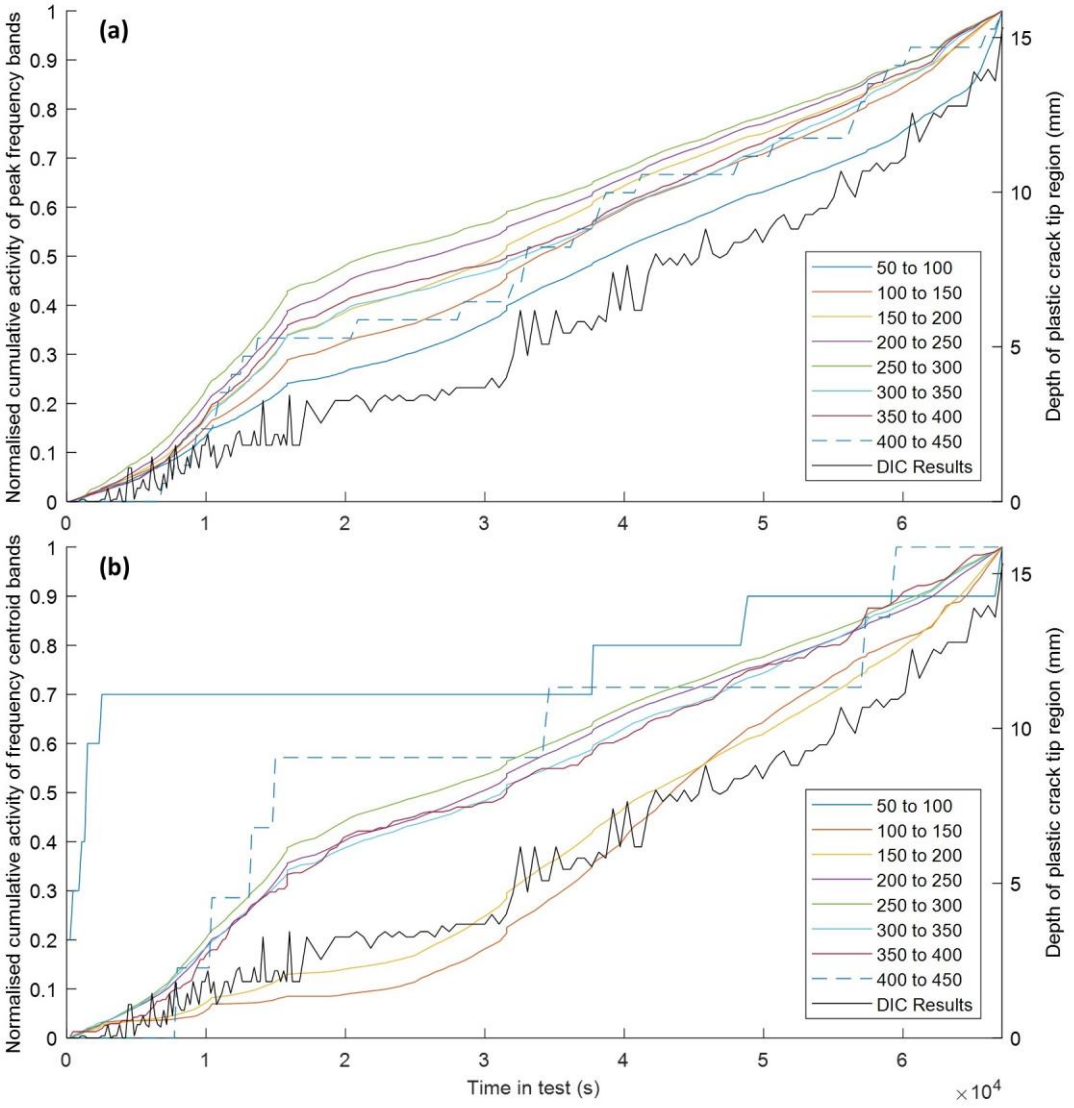

Figure 12: Cumulative activity of each 50 kHz band for the (a) peak frequency and (b) frequency centroid, for the 1.5 second long synthetic wavestreams

Though a number of the peak frequency bands display some semblance to the crack growth activity as determined from DIC, with notable features such as the decrease in the rate of activity at approximately 16,000 seconds into the test visible, it is the 50-100 kHz peak frequency band which bears the closest resemblance as it most accurately matches the changes in the gradient, i.e. rate of

activity, seen in the DIC data at all stages of the test. Referring to previous discussion, this is the peak frequency band which is thought to owe itself to crack-face rubbing [42,43,45]. With regard to the frequency centroid data, both the 100-150 and 150-200 kHz bands bear a good similarity to the crack growth activity as determined by DIC, though the 150-200 kHz band is the most comparable as it most closely matches the changes in the gradient. Again, this is the frequency centroid band which was predicted to have a connection to crack-face rubbing [46]. The 250-300 kHz frequency centroid band, previously highlighted as a potential indicator of crack growth activity, displays little significance and does not appear to exhibit any noticeable trends above and beyond the bulk of the other frequency centroid bands. It is possible that this is due to the fact that the sensors used are resonant over this range, thus they are likely to record a certain amount of energy at this frequency for all AE arriving at the sensor, no matter what the source. Thus, even if the 250-300 kHz frequency centroid band was related to the crack growth mechanism, since the occurrence of crack growth signals during fatigue is typically relatively low [45], they might not be able to drastically change the appearance of that frequency band above and beyond the trends dictated by the resonant-noise.

With regards to the comparison of the different length synthetic wavestreams to the conventional wavestreams, by plotting the cumulative activity of each peak frequency or frequency centroid band for all sets of data it was found that the trends in the 1.5, 1.0, and 0.5 second long synthetic wavestreams all bear a strong resemblance to those in the conventional wavestream, whereas the trends seen in the 0.25 second long synthetic wavestreams do not. This is exemplified in the plot of the normalised cumulative activity of the 300-350 kHz peak frequency band in Figure 13. Here the curves for the 1.5, 1.0 and 0.5 second long synthetic wavestreams are almost indistinguishable from the curve for the conventional wavestream at this scale, with average point-by-point errors of 1.3%, 1.3%, and 1.4% respectively, whereas the curve for 0.25 second long synthetic wavestreams clearly fails to display the same trends and has a larger average point-by-point error of 8.3% . This finding, along with the that in Figure 10, implies that there is enough data captured within the first 0.5 seconds of the recording to infer the same information, and thus draw the same conclusions about the state of the structure, as can be drawn from 1.5 seconds worth of data. To this extent the synthetic wavestreams have served their purpose of indicating an appropriate and more optimum wavestream recording length.

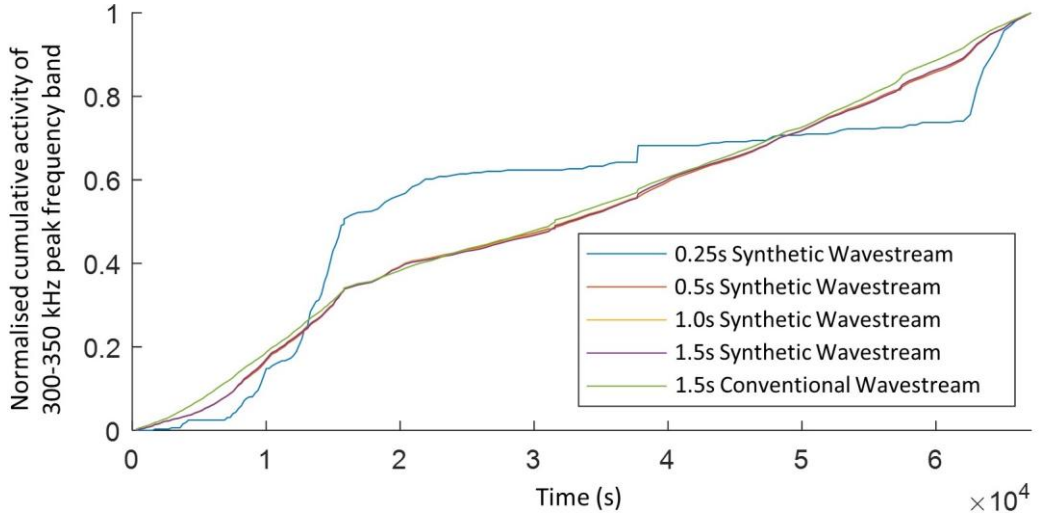

Figure 13: Cumulative activity of 300-350 kHz peak frequency band for each of the synthetic wavestreams and the conventional wavestream

Further to this, an argument could be made for the use of synthetic wavestreams as an alternative to conventional wavestreams in low power applications. The average number of hits recorded in each 1.5s long synthetic wavestream was 163, equating to 500,736 data points at a 2 MHz sampling rate. By contrast each 1.5s long wavestream is 3,000,000 data points for the same sampling rate. Thus, on average over the duration of this test, the synthetic wavestreams are just 16.7% of the size of the conventional wavestreams for the same effective recording length. Despite this, as seen throughout the results in this study, the conventional and synthetic wavestream data sets display the same trends, proving it is possible to gleam the same amount of beneficial information from just a fraction of the data. This could prove useful in scenarios where a low power wireless SHM system is needed, as smaller data sets would require less energy to store, process and transmit.

Conclusions

In this paper, the concept of adjoining hits to create synthetic wavestreams was introduced. Four sets of synthetic wavestreams with effective recording lengths of 0.25, 0.5, 1.0 and 1.5 seconds were created data recorded in a fatigue test of a notched cantilever steel beam. The trends in the synthetic wavestream data, namely the RMS amplitude, and the activity of peak frequency and frequency centroid bands, were compared with the trends in the 1.5 second long conventional wavestreams which were recorded during the same experiment. It was discovered that the 1.5, 1.0, and 0.5 second long synthetic wavestreams contained enough relevant data to mimic the trends found in the conventional wavestreams, but the 0.25 second long synthetic wavestreams were unable to do the same. Thus, the use of synthetic wavestreams as a tool for selecting an appropriate and optimal wavestream recording length was demonstrated. It is straightforward to picture how this approach could be used in a scoping study for a new AE SHM application; to conduct a trial experiment whilst collecting AE hit data and use that hit data to create a range of synthetic wavestreams to determine the optimal wavestream recording regime to use for the new application. Note that this study investigated four different length synthetic wavestreams in order to demonstrate the purpose, however, as the process of creating the synthetic wavestreams is script-automated it is possible to create a larger range and determine a more optimum recording length. Additionally, there is the potential to alter the time intervals between the creation of the synthetic wavestreams and further optimise the recommended wavestreaming regime. Ultimately, this study should be considered the first investigative step since it concerns a single application of the approach to a single failure mode on a controlled specimen, thus its effectiveness has yet to be proven on real world structures. Looking beyond the scope of synthetic wavestreaming purely as an optimising tool, it was found that on average the 1.5 second long synthetic wavestreams contained just 16.7% of the data in the 1.5 second long conventional wavestream, thus, synthetic wavestreaming presents itself as a potential data collection mechanism in its own right, which could have applicability for SHM systems where low power is a requirement.

With regards to using frequency data to track crack growth, the activity of the 50-100 kHz peak frequency and 150-200 kHz frequency centroid bands bore the closest resemblance to the crack growth rate as determined from DIC. Since both of these frequency bands have been suggested to relate to crack-face rubbing in numerous literature, it can said with reasonable certainty that this was the source mechanism responsible for the majority of the energy in these bands. It stands to reason that signals from crack face rubbing could be used as a descriptor of the crack length, as longer cracks have more area over which surface asperities can contact and friction can occur, so are likely to produce more AE due to crack face rubbing throughout loading than a shorter crack, especially under loading conditions with a low R-ratio as was the case in this experiment. High amplitude signals located as originating from the crack region, and thus thought to have originated from the crack growth

mechanism itself, were analysed spectrally. In agreement with other literature reporting on crack growth, the 300-400 kHz frequency band was prominent in these signals which resulted in these signals having a frequency centroid between 250-300 kHz. However, neither of these frequency bands displayed any distinct trends in relation to the crack growth activity above and beyond those found in the majority of the other frequency bands; this could be due to the low rate of occurrence of cracking signals relative to other emission sources meaning their influence on the activity of those frequency bands over the length of the experiment is diminished. Finally, the discretisation of the wavestreams into much smaller time windows for spectral processing was a valuable method of analysing frequency data that may have otherwise been lost in the entirety of the wavestream recording.

Funding

The authors received no financial support for the research, authorship, and/or publication of this article.

Declaration of conflicting interests

The Authors declare that there is no conflict of interest.

References

1. Martinez-Luengo M, Shafiee M. Guidelines and Cost-Benefit Analysis of the Offshore Wind Turbine Support Structures. Energies. 2019;12(1176).
2. Feldman K, Jazouli T, Sandborn P. A Methodology for Determining the Return on Investment Associated with Prognostics and Health Management. IEEE Trans Reliab. 2009;58(2):305–16.
3. Hölzel NB, Schilling T, Gollnick V. An Aircraft Lifecycle Approach for the Cost-Benefit Analysis of Prognostics and Condition-based Maintenance based on Discrete-Event Simulation. In: Annual Conference Of The Prognostics And Health Management Society. 2014. p. 435–50.
4. Pollock AA. Acoustic Emission Inspection. In: Metals Handbook. Ninth Edit. ASM Inernational; 1989. p. 278–94.
5. Mistras Group Inc. PAL Provides Severn River Crossing Bridge Long-term Cable Evaluation. Newsroom [Internet]. 2008 Jul; Available from: https://www.mistrasgroup.com/company/newsroom/2008/07/01/pal-provides-severn-river-crossing-bridge-long-term-cable-evaluation/
6. TechKnowServ Corp. Recertification of Tube Trailers using Acoustic Emission Testing [Internet]. 2019 [cited 2019 Jun 20]. Available from: https://www.techknowserv.com/blog/recertification-of-tube-trailers-using-acoustic-emission-testing/
7. FIBA Techologies. Acoustic Emission Testing (AET) [Internet]. Services. 2018 [cited 2019 Jun 20]. Available from: https://www.fibatech.com/services/acoustic-emission-testing-aet/
8. Lage Y. Detection of Fatigue Crack Initiation on Welded Joints [Internet]. TWI Insights. 2019 [cited 2019 Jun 20]. Available from: https://www.twi-global.com/media-and-events/insights/detection-of-fatigue-crack-initiation-on-welded-joints-using-acoustic-emission-monitoring
9. SSA Acoustic & Specialised Inspections. Permanent Online Monitoring (Acoustic Emission) [Internet]. Services. 2017 [cited 2019 Jun 20]. Available from: https://ssaacoustic.com/services/permanent-online-monitoring-acoustic-emission-2/
10. Mistras Group Inc. Micro-SHM product data sheet [Internet]. 2017 [cited 2019 Jan 20]. Available from:

https://www.physicalacoustics.com/content/literature/small_systems/Micro_SHM_Product_Data_Sheet.pdf

11. Tang X, Wang X, Cattley R, Gu F. Energy Harvesting Technologies for Achieving Self-Powered Wireless Sensor Networks in Machine Condition Monitoring : A Review. J Sen. 2018;18.
12. Pearson MR, Eaton MJ, Pullin R, Featherston CA. Energy Harvesting for Aerospace Structural Health Monitoring Systems. J Phys Conf Ser. 2012;382(August).
13. Mascaro B, Gibiat V, Bernadou M, Esquerre Y. Acoustic Emission of the Drilling of Carbon/Epoxy Composites. In: Forum Acusticum, Budapest, Hungary. 2005. p. 2823–7.
14. Eaton MJ, Pearson MR, Byrne C, Prickett P, Pullin R, Holford KM, et al. Ensuring Drilli Quality in Composite Materials Using Acoustic Emission. 2014;(June):22–6.
15. Tan CK, Irving P, Mba D. A Comparative Experimental Study On The Diagnostic And Prognostic Capabilities Of Acoustics Emission , Vibration And Spectrometric Oil Analysis For Spur Gears. Mech Syst Signal Process. 2007;21:208–33.
16. Toutountzakis T, Mba D. Observations of Acoustic Emission activity during gear defect diagnosis. NDT E Int. 2003;36(7):471–7.
17. Al-Ghamdi AM, Zhechkov D, Mba D. The use of Acoustic Emission for bearing defect identification and estimation of defect size. In: The 26th European conference on Acoustic Emission testing. 2004.
18. Elforjani M, Mba D. Detecting Natural Crack Initiation and Growth in Slow Speed Shafts With the Acoustic Emission Technology. Eng Fail Anal [Internet]. 2009;16(7):2121–9. Available from: http://dx.doi.org/10.1016/j.engfailanal.2009.02.005
19. Elforjani M, Mba D. Detecting the Onset, Propagation and Location of Non-artificial Defects in a Slow Rotating Thrust Bearing With Acoustic Emission. Insight Non-Destructive Test Cond Monit. 2008;50(5):264–8.
20. Elforjani M, Mba D. Accelerated Natural Fault Diagnosis in Slow Speed Bearings With Acoustic Emission. Eng Fract Mech [Internet]. 2010;77(1):112–27. Available from: http://dx.doi.org/10.1016/j.engfracmech.2009.09.016
21. Eftekharnejad B, Addali A, Mba D. Shaft Crack Diagnostics in a Gearbox. Appl Acoust [Internet]. 2012;73(8):723–33. Available from: http://dx.doi.org/10.1016/j.apacoust.2012.02.004
22. Pullin R, Clarke A, Eaton MJ, Pearson MR, Holford KM. Identification of the Onset of Cracking in Gear Teeth Using Acoustic Emission. J Phys Conf Ser. 2012;382(1):12050.
23. Holford K, Eaton M, Clarke A, Pearson M, Featherston CA, Pullin R. Approaches to Acoustic Emission Monitoring With Applicability to Key Components in Wind Turbines. In: Proceedings of 9th International Workshop on Structural Health Monitoring. Stanford University, USA; 2013.
24. Pullin R, Pearson MR, Eaton MJ, Featherston CA, Holford KM, Clarke A. Automated Damage Detection in Composite Components Using Acoustic Emission. Key Eng Mater. 2013;569–570:80–7.
25. Pullin R, Pearson MR, Eaton MJ, Featherston CA, Holford KM, Alastair C. Automated Damage Detection in Composite Components Using Acoustic Emission. Key Eng Mater. 2013;Volumes 56:80–7.
26. Zhang L, Ozevin D, He D. A Method to Decompose the Streamed Acoustic Emission Signals for Detecting Embedded Fatigue Crack Signals. J Appl Sci. 2017;8(1).
27. Eaton MJ, Pullin R, Holford KM. Acoustic Emission Source Location in Composite Materials Using Delta T Mapping. Compos Part A Appl Sci Manuf [Internet]. 2012;43(6):856–63. Available

from: http://www.scopus.com/inward/record.url?eid=2-s2.0-84860181606&partnerID=40&md5=e2d23910c45bd2d492d8f26f4c0f6a97

28. McCrory JP, Pullin R, Pearson MR, Eaton MJ, Featherston CA, Holford KM. Effect of Delta-T Grid Resolution on Acoustic Emission Source Location in GLARE. In: 30th European Conference on Acoustic Emission Testing & 7th International Conference on Acoustic Emission. 2012.
29. Baxter MG, Pullin R, Holford KM, Evans SL. Delta T Source Location for Acoustic Emission. Mech Syst Signal Process [Internet]. 2007;21(3):1512–20. Available from: http://www.sciencedirect.com/science/article/pii/S0888327006001178
30. Pearson MR, Eaton M, Featherston C, Pullin R. Improved Acoustic Emission Source Location During Fatigue and Impact Events in Metallic and Composite Structures. Struct Heal Monit. 2017;16(4).
31. P. L. Reu, B. R. Rogillio GWW. Crack Tip Growth Measurement Using Digital Image Correlation. In: Experimental Analysis of Nano and Engineering Materials and Structures. Dordrecht: Springer; 2007. p. 555.
32. H.J.K. Lemmen, R.C. Alderliesten, R. Benedictus, J.C.J. Hofstede RR. The power of Digital Image Correlation for detailed elastic-plastic strain measurements. In: WSEAS International Conference on Engineering Mechanics. Heraklion, Crete Island, Greece; 2008.
33. Roylance D. Mechanical Properties of Materials. MIT; 2008.
34. Irwin GR, Paris PC, Tada H. The Stress Analysis of Cracks Handbook. Third, editor. American Society of Mechanical Engineers; 2000.
35. Cox, B.N., Pardee, W.J., Morris WL. A Statistical Model of Intermittent Short Fatigue Crack Growth. Fatigue Fract Eng Mater Struct. 1987;9(6):435–55.
36. Ritchie RO. Mechanisms of Fatigue-crack Propagation in Ductile and Brittle Solids. Int J Fract. 1999;100:58–83.
37. Hobson PD. The Growth of Short Fatigue Cracks in Medium Carbon Steel. University of Sheffield; 1985.
38. Davidson DL. How Fatigue Cracks Grow, Interact With Microstructure, and Lose Simulate. Fatigue Fract Mech. 1997;27:287–300.
39. Romaniv ON, Kirillov KI, Zima Y V., Nikiforchin GN. Relationship Of Acoustic Emission To The Kinetics And Micromechanism Of Fatigue Failure Of High-strength Steel With A Martensitic Structure. Sov Mater Sci. 1987;23(2):156–60.
40. Scruby CB, Jones C, Titchmarsh JM, Wadley HNG. Relationship Between Microstructure and Acoustic Emission in Mn-Mo-Ni A533B Steel. Met Sci. 1981;(June).
41. Ono K. Current Understanding of Mechanisms of Acoustic Emission. J Strain Anal. 2005;40(1).
42. Bhuiyan Y, Giurgiutiu V. The Signatures of Acoustic Emission Waveforms From Fatigue Crack Advancing in Thin Metallic Plates. Smart Mater Struct. 2018;27(015019).
43. Ono, K., Wu JY. Pattern Recognition Analysis of Acoustic Emission From Fatigue of 2024-T4 Aluminum. In: Progress in Acoustic Emission. Tokyo; 1996. p. 237–42.
44. Aggelis DG, Kordatos EZ, Matikas TE. Monitoring of Metal Fatigue Damage Using Acoustic Emission and Thermography. J Acoust Emiss [Internet]. 2011 Mar [cited 2019 Jan 11];29. Available from: https://linkinghub.elsevier.com/retrieve/pii/S0093641311000139
45. Sison M, Jr JCD, Lozev MG, Clemeña GG. Analysis of Acoustic Emissions from a Steel Bridge Hanger. J Res Nondestruct Eval. 1998;10(3):123–45.
46. Pollock AA, Yu JP, Ziehl P. AE Observations During Cyclic Testing of A572 Steel Laboratory

Specimens 2. In: 30th European Conference on Acoustic Emission Testing & 7th International Conference on Acoustic Emission. Granada; 2012.

47. Buttle, D.J., Scruby CB. Characterization of Fatigue of Aluminum Alloys by Acoustic Emission, Part I–II. J Acoust Emiss. 1990;9(4).

48. Crivelli D, Mccrory J, Miccoli S, Pullin R, Clarke A. Gear Tooth Root Fatigue Test Monitoring With Continuous Acoustic Emission : Advanced Signal Processing Techniques for Detection of Incipient Failure. Struct Heal Monit. 2017;17(3):423–33.